Appl Phys B (2010) 101: 15–22
DOI 10.1007/s00340-010-4185-5

Applied Physics B
Lasers and Optics

Energy scaling-up of stable single filament

B. Alonso · O. Varela · I.J. Sola · J. San Román · A. Zaïr · C. Méndez · L. Roso

Received: 18 June 2010 / Revised version: 15 July 2010 / Published online: 26 August 2010

Abstract The influence of the input pulse chirp and energy on the filamentation process is studied. Output beam profiles, spectra and energies were systematically measured by changing the pulse chirp for different input energies. A map of the different energy-chirp regions was compiled. It shows that high-energy stable single filament can be obtained by using chirped input pulses, allowing the scaling-up of the energy throughput in the filament. Moreover, under high-energy regimes nonlinear effects induced by chirped pulses could produce pulse post-compression.

1 Introduction

The self-guiding propagation of light at high power (referred to as filamentation) [1] is a phenomenon that has been intensively studied in recent years. It arises from the balance between the tendency of the beam to collapse produced by the self-focussing effect due to the Kerr effect and the defocussing caused by the subsequently induced plasma. This peculiar propagation regime has several applications, covering an important range of topics such as the propagation of filaments for testing different atmospheric conditions [2], virtual antennas [3], remote analysis of materials by Laser-Induced Breakdown Spectroscopy (LIBS) [4], and even the control of lightning guiding [5], among others.

B. Alonso · O. Varela · I.J. Sola (✉) · J. San Román · A. Zaïr
Departamento de Física Aplicada, Facultad de Ciencias, Universidad de Salamanca, 37008 Salamanca, Spain
e-mail: ijsola@usal.es

C. Méndez · L. Roso
Centro de Láseres Pulsados Ultracortos Ultraintensos, CLPU, 37008 Salamanca, Spain

Another application in which filamentation is especially useful is the post-compression of laser pulses. Some years ago, ultra-short pulses were obtained using filamentation and phase compensation by means of chirped mirrors [6]. In standard setups, the output energy is typically of some hundreds of μJ or a few mJ, very similar to the post-compression technique in which spectral broadening is obtained by coupling the beam in a hollow fibre filled with gas [7]. The limitation to more energetic outcomes arises from changes in the physical process when more energy is used (in the case of hollow fibres, the limitation derives from the ionisation of the medium, and in the case of filamentation it is due to the multi-filamentation regime). Since advances in femtosecond lasers now provide high-power laser pulses with energies exceeding these limits, the adaptation of the post-compression scheme to these high-energy sources remains a challenge. One of the first setups that attempted to overcome the present limitation was based on hollow-fibre post-compression, using a gas gradient in order to avoid the formation of plasma: outputs of 5 mJ/9 fs and 2.5 mJ/5 fs were obtained [8, 9]. Also more recently, hollow planar waveguide setups have been used, obtaining 2 mJ/12 fs pulses [10] and later 7.6 mJ/11.6 fs [11]. In addition, the role of incoming pulse polarisation in filamentation has been explored. It has been shown that it is possible to compress a pulse with an initial circular polarisation down to 15 fs by using filamentation post-compression [12]. Regarding the energy scaling-up issue, one of the main advantages of elliptical or circular polarised beam filamentation is that higher output energies can be reached successfully, as we have shown very recently in [13], maintaining supercontinuum generation, and hence affording few-cycle pulses. This scheme has subsequently been applied to hollow-fibre post-compression [14]. The increasing number of scientific contributions devoted to the adaptation of pulse

post-compression techniques to high-energy regimes illustrates the interest in this issue.

A possible alternative strategy for overcoming the limitations of the nonlinear processes used for spectral broadening in femtosecond pulse post-compression is to avoid overly high powers by chirping the input pulses. For example, in post-compression assisted by filamentation, the power could be maintained below the critical value for multi-filamentation. Previous works have studied the effect of input chirp on the self-guiding process. First, input chirp allows the control of the self-focussing collapse corresponding to the beginning of filamentation and its length [15–17]. Thus, negative chirps lead to longer self-guiding lengths owing to the existence of more focussing-defocussing cycles [15, 16]. Indeed, this property can be used in atmospheric propagation to control filamentation [18, 19]. In the spectral domain, it has been shown that slightly positive input chirps are able to produce higher degrees of spectral broadening [20], allowing better post-compression because of the SPM-induced red chirp [21]. In contrast, slightly negative input chirps produce less efficient spectral broadening or even spectral narrowing because of the nature of the abovementioned positive chirping (the input pulse chirp now is opposite that induced by the SPM effect), although this spectrum reshaping can lead to pulses shorter than the original one [22]. Therefore, the input pulse chirp plays a key role in the filamentation process.

Here we studied the effect of input chirp on the generation of a stable single filament across a broad range, searching for the possibility of scaling-up the energy transmitted along the filament, while at the same time maintaining a stable single filament. With this aim, the work is structured as follows. First, the experimental setup is described and systematic scans on input energy and chirp are shown, measuring spectra, spatial mode profiles, and energies at the output. These scans allow us to follow the diverse propagation regimes and to map the different situations. From this general map, the conditions for the energy rescaling can be obtained. In particular, an energy-chirp relationship is inferred in order to obtain stable high-energy single filaments with the necessary requirements for implementing high-energy post-compression.

2 Setup and results

For the experimental setup, a Spectra Physics Ti:sapphire laser system delivering 120 fs pulses under the Fourier limit condition (central wavelength at 795 nm, FHWM = 9 nm), with a spatial distribution of 9 mm in diameter (FWHM), a repetition rate of 10 Hz and energy up to 7 mJ after a 6 mm aperture iris was used. This iris was used in order to accommodate the input spatial profile to an appropriate filamentation process. The beam was focused in air by means of a lens with a focal length of 1.5 m. Once the beam had propagated, at 3 metres after the nominal focus, the resulting beam was characterised. Spectra were measured on-axis with a spectrometer (AvaSpec 2048 from Avantes). The spatial profile of the beam at the same position was obtained by means of a CCD camera.

The spectra, energies and spatial profiles of the resulting beams were monitored for different energies and chirps of the input pulses. Input energy was scaled using a variable attenuator based on a half-wave plate and a polariser installed before the laser pulse compressor, while chirp was modified by changing the distance between the gratings of the laser compressor. This modification directly affects the quadratic order (the group delay dispersion, GDD) of the laser pulse phase.

The dependence of the input pulse chirp on the grating position was characterised using the SHG FROG technique (in its single-shot version, a GRENOUILLE 50 from Swamp Optics, which is able to measure pulses from 50 fs to 500 fs). The GDD was measured and the results matched well the expected linear dependence on the grating position. Since it was possible to introduce bigger chirps than those measured within the range of our pulse reconstruction device, the experimental fitting was carefully compared with the theoretical dependence of the compressor, taking into account its parameters. According to this calibration, it was possible to introduce an input GDD range from -132640 fs^2 to $+60638$ fs^2.

Input chirp scans within the available range were performed for different input energies, from 1 mJ to 7 mJ, after the input iris. The results are shown in Figs. 1 to 4, each including two different subplots. The top image (a) shows the spectral effects for different input chirps. In particular, it shows the on-axis output spectra as a function of the input GDD values. In contrast, image (b) shows the output energy measured through an output iris as a function of the input GDD at 3 m after the nominal focus. The x-axis shows in the lower side the input GDD obtained from the calibration, while in the upper side the corresponding powers are shown. The output iris was closed to select the filament inner core (3.3 mm at 3 m after the nominal focus). The criteria used to consider the inner core were the spatial distribution, selecting the central mode generated by the filament, and the spectrum, which must be constant along the whole selection [23]. The evolution of the filament central mode energy while the chirp is scanned, together with the spatial profile observed, allows the identification of different propagation regimes in a similar way to Ref. [24]. Finally, in order to complete the analysis, spatial distributions were measured for all the energy-chirp cases. Some of the most relevant cases have been plotted with a view to offer readers a more comprehensive view.

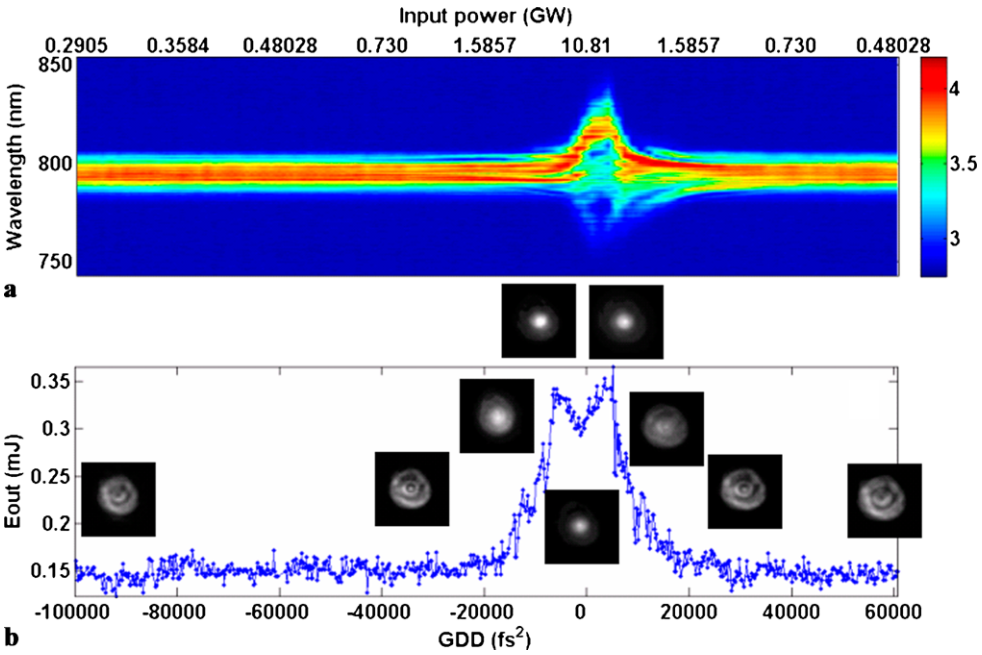

Fig. 1 Spectra on logarithmic scale (**a**) and output energies (**b**) depending on the input GDD. Attached images are the spatial mode distributions under the most relevant conditions. $E_{\text{input}} = 1$ mJ. Input power ticks correspond to the GDD values of the lower scale

The first case analysed corresponds to an input energy of 1 mJ. This is a typical value used in post-compression setups since, with the usual gaseous media (N_2, Ar, Ne, etc.) and the usual experimental conditions; the intensity is not high enough to enter the multi-filamentation regime. Spectral broadening can only be observed for low values of the input chirp (i.e. the highest input power). This can also be compared with the output spatial profiles. For high negative chirp values (i.e., low input powers), neither spectral broadening nor central mode formation was observed. Upon decreasing the negative GDD (-37565 fs^2), the first signature of nonlinearity was observed since the diffraction pattern changed slightly: a central maximum appeared while in linear propagation a minimum was seen at the centre. This is the signature of the self-focussing of the beam induced by the Kerr effect. However, this nonlinearity was not strong enough to induce changes in the spectrum.

Shorter input pulses (GDD from -26500 fs^2 to -4831 fs^2) produced important spatial effects, deleting the spatial diffraction pattern and replacing it by an incipient central mode. Additionally, a slight spectral narrowing was observed. This was due to the fact that the negative input chirp was opposite the SPM-induced red chirp. This behaviour has already been observed in filaments [20, 22]. The creation of the central mode also involved a rise in the energy measured through the output iris. This transition region (as well as that observed in positive chirp regions, discussed below) can be identified with a propagation regime where the antagonistic roles are played by the Kerr effect, as a focussing mechanism, and diffraction as a defocussing mechanism, since the ionisation is not strong enough to have a relevant effect [25].

By further decreasing the negative chirp, thus raising the input power, the nonlinear effects appeared more clearly. For a GDD of -4831 fs^2, a maximum in the output energy plot (Fig. 1b) was observed, while a well-defined central mode was formed. A small spectral broadening also appeared, since the chirp induced by the SPM effect may be enough to compensate the negative input GDD. When the input pulses were Fourier-limited, the spectral broadening was higher and only a single spatial mode was observed because the intensity was not high enough to generate multi-filaments. When positive chirp was added to the input pulses, spectral broadening continued to increase. This is consistent with previous experimental observations [20] and the expected behaviour of SPM for a chirped pulse (i.e. a higher broadening for positive chirp due to its positive chirping nature). The maximum broadening appeared at a positive chirp value, where a maximum in the output energy was also seen, observing a well-defined spatial mode. Although the two output energy maxima appeared at a similar absolute GDD value, the effect on spectral broadening was clearly different, owing to the effect of the sign of the chirp on the SPM and the nonlinear propagation of the light. Another interesting observation was that the spectral broadening was red-shifted in general. This shift is caused by the Raman effect while propagating in air. The observed spectral broadening and red shift is very similar to the reported in [26], while in that work the light did not propagate in filamentation regime. This confirms the impression that the SPM is the main mechanism behind the spectral mechanism observed in our case.

Higher input energies changed the dynamics of the light propagation. Figures 2 to 4 show the corresponding scans at

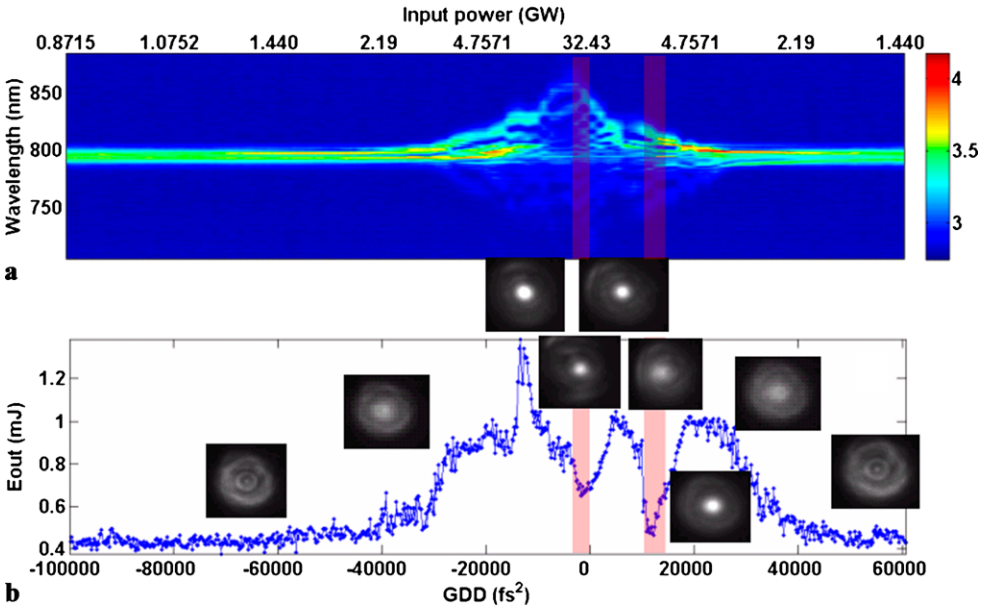

Fig. 2 Spectra at logarithmic scale (**a**) and output energies (**b**) depending on the input GDD. Attached images are the spatial mode distributions under the most relevant conditions. $E_{\text{input}} = 3$ mJ. Input power ticks correspond to the GDD values of the lower scale

3 mJ, 5 mJ and 7 mJ respectively. In Fig. 2 (corresponding to an input energy of 3 mJ), two regions of instabilities arose at around GDD $= 0$ fs^2 and GDD $= +12120$ fs^2, denoted by red shading. In the present work, we use the term 'instability regions' to refer to those including different behaviours of the beam, having in common the loss of a symmetric stable single filament spatial pattern. This includes cases such as asymmetric single filament formation (typically, the central mode is spatially shifted), unstable shot-to-shot distributions, and multi-filamentation. In the particular case of 3 mJ, the instabilities were due mainly to asymmetric single filament spatial patterns. In the output energy measures two minima were observed, corresponding to the spatial shift of the central mode. Thus, we obtained three chirp regions in which a stable centred single filament was obtained: one for negative GDD and two for positive GDD. It is also interesting to note that the broadening was higher for negative chirp than for the positive case (Fig. 2a). This kind of behaviour was contrary to that observed with low energy (1 mJ) in Fig. 1a. A possible explanation lies in the compensation of the input negative chirp by the dispersion due to filamentation propagation (mainly SPM). The step structure of the evolution of the spectra with the negative GDD (Fig. 2a) is suggestive of such a process.

The behaviour of the propagation depending on the GDD changed again for the higher-energy cases. Figures 3 shows the scans performed for 5 mJ. Now, the regions of instabilities have broadened and merged into a single large one. In fact, there were again two main stable single filament regions (corresponding to positive and negative GDD). Upon studying the spectral effects, a greater degree of broadening was observed for positively chirped pulses, whose spectra afforded typical SPM structures. Although we did not include any stability region at low GDD values (cases of higher input power) in Fig. 3, inside the shaded regions, at very specific values of the parameters, stable single filaments can be found (at both, positive and negative GDD), coinciding with some of the output energy peaks. Finally, the evolution of the output energy and spectra when changing the chirp for higher input energy cases (7 mJ) was found to be very similar to that observed for 5 mJ (Fig. 4).

In order to gain a more general view of the cases studied, the behaviour of light propagation is summarised in Fig. 5. It shows a map of the input power as a function of the input energy, showing the diverse regions of propagation. The input power values were obtained from the compressor calibration and the measured energy. It should be stressed that we set the power to be negative for negative GDD cases only for plotting purposes. The regions were determined combining the observations of output energy and the spatial profile. The white colour denotes the regions where no data are available with our laser system and compressor. These regions are located at the high-power regime (since the maximum input power is given by the input energy and the minimal pulse duration) and at the low-power regime (because the minimum input power is limited by the maximum chirp introduced to the input pulse, and it is given by the compressor range).

As mentioned before, pulses with low input powers did not generate any nonlinear effect (deep blue region), conserving the input spectrum and showing a diffractive spatial pattern produced by the light passing through the input iris. Non-linear effects began to affect the light propagation for higher input powers (blue region). Thus, the diffractive spatial pattern displays a central maximum instead of the minimum expected for linear propagation. In the cases observed,

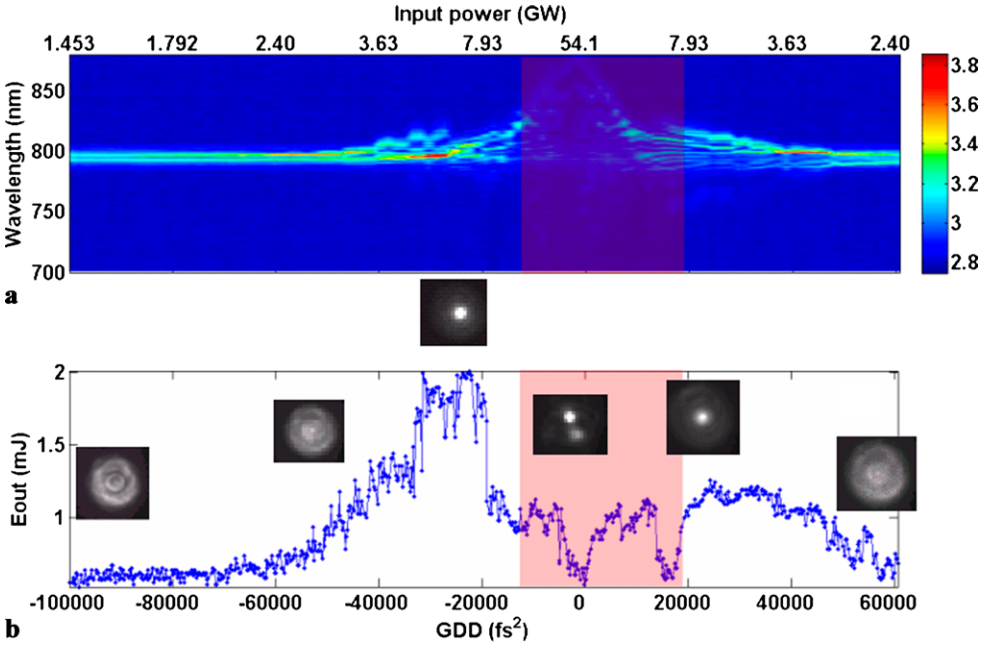

Fig. 3 Spectra at logarithmic scale (**a**) and output energies (**b**) depending on the input GDD. Attached images are the spatial mode distributions under the most relevant conditions. $E_{\text{input}} = 5$ mJ. Input power ticks correspond to the GDD values of the lower scale

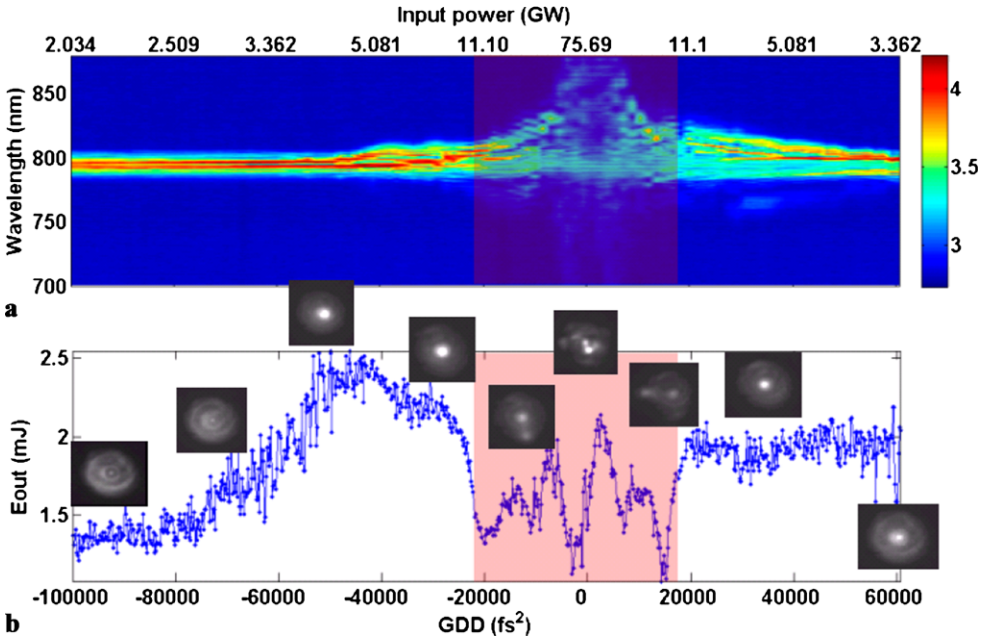

Fig. 4 Spectra at logarithmic scale (**a**) and output energies (**b**) depending on the input GDD. Attached images are the spatial mode distributions under the most relevant conditions. $E_{\text{input}} = 7$ mJ. Input power ticks correspond to the GDD values of the lower scale

the beginning of this nonlinear change appeared at the range of 0.6 GW–1.17 GW, just below the critical power of air $P_{\text{cr}} \approx 4$ GW. Within the power range of very few GW, major changes were observed in the spatial profile. While the input power increased the nonlinear diffractive pattern evolved towards the formation of an incipient central mode. At the same time, some spectral changes were observed, especially with positive chirp. This regime marks the transition to a new region of behaviour, where the single filament profile appears fully developed.

For input powers above the critical power, from a few GW to some few tenths of a GW, depending on the sign of the chirp and on the input energy, the beam propagated in the form of a stable single filament. In the cases studied, apart from slight variations in the values, qualitatively two regions of stability (at positive and negative input GDD) arose in this power range. In the map (Fig. 5) the conditions where a stable single filament presenting a symmetric spatial distribution was obtained are marked in green. Finally, the red denotes the instability region, including, as previously com-

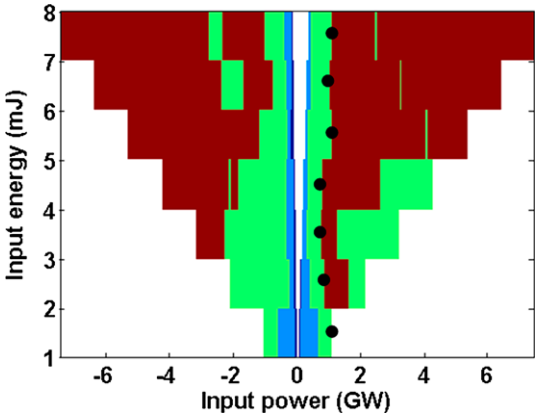

Fig. 5 Map of the behaviour of light propagation depending on the input energy and power (obtained by chirping the input pulses). Negative input power means that the input pulses were negatively chirped. Linear regions (*deep blue*), nonlinear regions (*blue*), single filamentation central mode (*green*) and unstable structures ranging from asymmetric distributions to multi-filamentation (*red*) are shown. No data are available for the white regions. *Black circles* mark the conditions used for energy scaling-up of filaments for post-compression applications

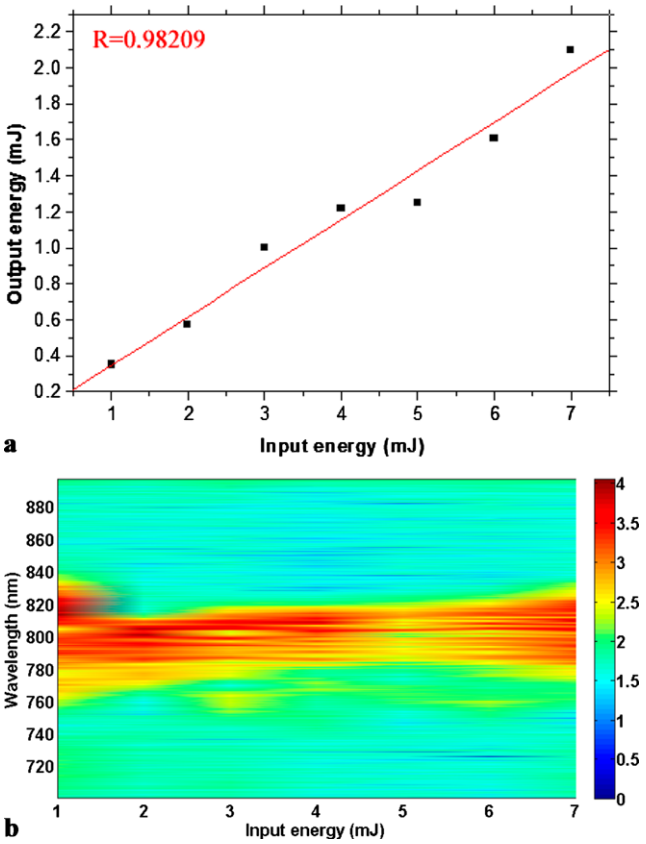

Fig. 6 (**a**) Central mode output energy as a function of the input energy for some particular GDD/energy pairs described in the text and marked with black circles in Fig. 5. (**b**) Spectral broadening (logarithmic scale) depending on the energy for the same GDD/energy pairs

mented, deformations of the central mode of the filament, unstable distributions, and multi-filamentation. It is very interesting to note that the stability region was observed not only in the above-mentioned range of some GW. For input powers ranging from 2 to 4 mJ, a third stability region was observed at higher input powers with positive GDD. For higher input energies (5 mJ to 7 mJ) this region evolved towards isolated and localised ranges of input GGD values (above the 20 GW level), located within broader instability regions. It may be considered as a remainder of the former stable region observed at lower input energies. Similar behaviour was observed for negative input chirp. The nature of these high-power input stability regions is not very clear. A possible explanation could be that they might arise under some very precise conditions in which the different contributions to the spectral phase would compensate one another. Currently we are studying the pulse time reconstruction according to the input conditions, and this may help to understand the mechanism responsible for this effect.

As a general conclusion of Fig. 5, for a given high-energy input, appropriate chirping of the pulse can be found, yielding the formation of a single high-energy filament and thus preventing the formation of multi-filaments.

3 High-energy chirped pulse single filament and its possible application to high-energy post-compression

Since we were searching for a robust and reproducible scheme of scaling-up the throughput energy in the process of stable single filament formation, we focused on the stable regions in Fig. 5 (corresponding to positive and negative GDDs), in which a single filament was formed. In particular we selected the region where a single filament was obtained at low power and positive GDD (the selected input energy-GDD pairs appear as black circles in Fig. 5). This selection was made bearing in mind that the equivalent power region with negative GDD exhibits lower spectral broadening and that the cases with higher input power and stable single filament formation appear in a much more critical parameter regime.

Spatially, the distributions of the observed modes were very similar. When the output central mode was selected and the output energy was measured, some conclusions were obtained. In Fig. 6a we show the central mode output energy obtained for these particular input energy-GDD pairs *versus* the input energy. It is interesting to note the very linear behaviour (the transmission rate is around 30% in all cases), reaching the 2.1 mJ level for the highest input energy available (7 mJ) and showing a scaling-up of the filament energy. This behaviour also appeared in the rest of the cases within the low-power single filament region for positive input GDDs and analogous cases at negative input GDDs. In sum, by adjusting the input pulse chirp to the incoming energy, it is possible to bypass the multi-

filamentation regime, obtaining multi-millijoule single filaments and, more importantly, a linear trend toward even more energetic filaments if the input energy available is high enough.

However, the application of this phenomenon to high-energy post-compression also requires an important nonlinear broadening of the spectrum to ensure a potential compression. The selected energy-GDD pairs showed a maximum in broadening as compared with the other combinations with positive input GDD, and in general the negative input GDD options showed a lower spectral broadening. Figure 6b shows the spectra (logarithmic scale) corresponding to the output energies from Fig. 6a. For low energies (1 mJ), spectra broadened by about 30 nm were obtained. When the energy increased (2–3 mJ) and positive chirp was needed to maintain the stability of the single filament, the broadening was still present, but it was less pronounced. Nevertheless, when the energy-chirp pair increased, the spectral broadening increased. For 7 mJ-input pulses (2.1 mJ output), the broadened spectrum was very similar to the former one of 30 nm (see Fig. 6b). Again, therefore, not only did the results for the 7 mJ show a spectral broadening comparable to the 1 mJ situation but, in addition, the trend was for this broadening to increase with the energy and the input chirp. Accordingly, the low input power (4 GW–10 GW) positive chirped range was the most suitable potential region for generating high-energy and spectral broadening pulses for post-compression.

These results open the door to the scaling-up of post-compression energy for a given setup. Simply by interplaying energy and chirp, without making any other changes in the experimental configuration, the energy carried by a stable single filament can be adapted to a higher-energy regime while the spectral broadening is, at least, conserved. In the present work we have controlled the GDD by changing the compressor grating distance; a more sophisticated spectral phase control may be introduced for further improvement (a previous attempt of pulse shaping applied to filamentation property optimisation is presented in Ref. [27]).

In addition, the input pulse chirping could be applied together with other techniques, such as the use of circular polarised input pulses [13], in order to obtain further results on energy scaling-up. A possible limitation of the scaling-up obtained with the use of chirped input pulses may appear when the input energy is so high that it will require very stretched input. As commented in Ref. [28, 29], at those conditions the absorption of the beam energy by the plasma generated will increase because of the inverse Bremsstrahlung, leading to an exponential increase in plasma density, affecting the filament regime. However within our measurement range (up to 7 mJ, 2 ps stretched input pulses) we have not observed such an effect.

4 Conclusions

In this work we systematically analysed the behaviour of beam propagation, scanning the incoming pulse energy and chirp over a broad range. Different regions of behaviour were identified and mapped, including nonlinear propagation, and single and multiple filamentation, correlating the measurements implemented. Thus, the values of the input energy and chirp and their balance are discussed.

Some of the observed regions seem to be good candidates for high-energy stable single filamentation and its further application to high-energy post-compression. In particular, the appropriate positive chirping of high-energy input pulses allows the output pulse energy to be scaled-up, preventing the formation of multi-filaments and conserving the transmission factor and the spectral broadening. Not only high-energy stable single filaments were observed (up to 2.1 mJ), but also, and most encouragingly, the linear dependence allowed even higher energies to be obtained. No limitation to the scaling-up was observed experimentally. Spectral phase compensation would lead to compression of these high-energy pulses.

Acknowledgements We acknowledge support from Spanish Ministerio de Ciencia e Innovación through the Consolider Program SAUUL (CSD2007-00013) and Research project FIS2009-09522, from Junta de Castilla y León through the Program for Groups of Excellence (GR27) and grant SA002B08, and from the EC's Seventh Framework Programme (LASERLAB-EUROPE, grant agreement n° 228334). B. Alonso and I.J. Sola acknowledge the support from the Spanish Ministerio de Ciencia e Innovación through the "Formación de Profesorado Universitario" and the "Ramón y Cajal" grant programs respectively. The authors acknowledge L. Bañares, from the Universidad Complutense de Madrid, for lending the GRENOUILLE 50 and the support from the Centro de Laseres Pulsados, CLPU, Salamanca, Spain.

References

1. A. Braun, G. Korn, X. Liu, D. Du, J. Squier, G. Mourou, Opt. Lett. **20**, 73 (1995)
2. J. Kasparian, M. Rodríguez, G. Méjean, J. Yu, E. Salmon, H. Wille, R. Bourayou, S. Frey, Y.-B. André, A. Mysyrowicz, R. Sauerbrey, J.-P. Wolf, L. Wöste, Science **301**, 61 (2003)
3. G. Méchain, A. Mysyrowicz, M. Depiesse, M. Pellet, in *Technologies for Optical Countermeasures II; Femtosecond Phenomena II; and Passive Millimetre-Wave and Terahertz Imaging II*, ed. by D.H. Titterton, S.M. Kirkpatrick, R. Stoian, R. Appleby, J.M. Chamberlain, K.A. Krapels, vol. 5989 (SPIE, Bellingham, 2005), p. 5989
4. K. Stelmaszczyk, P. Rohwetter, G. Méjean, J. Yu, E. Salmon, J. Kasparian, R. Ackermann, J.-P. Wolf, L. Wöste, Appl. Phys. Lett. **85**, 3977 (2004)
5. J. Kasparian, R. Ackermann, Y.-B. André, G. Méchain, G. Méjean, B. Prade, P. Rohwetter, E. Salmon, K. Stelmaszczyk, J. Yu, A. Mysyrowicz, R. Sauerbrey, L. Wöste, J.-P. Wolf, Opt. Express **16**, 5757 (2008)
6. C.P. Hauri, W. Kornelis, F.W. Helbing, A. Heinrich, A. Couairon, A. Mysyrowicz, J. Biegert, U. Keller, Appl. Phys. B **79**, 673 (2004)

7. M. Nisoli, S. De Silvestri, O. Svelto, R. Szipöcs, K. Ferencz, Ch. Spielmann, S. Sartania, F. Krausz, Opt. Lett. **22**, 522 (1997)
8. A. Suda, M. Hatayama, K. Nagasaka, K. Midorikawa, Appl. Phys. Lett. **86**, 111116 (2005)
9. S. Bohman, A. Suda, M. Kaku, M. Nurhuda, T. Kanai, S. Yamaguchi, K. Midorikawa, Opt. Express **16**, 10684 (2008)
10. J. Chen, A. Suda, E.J. Takahashi, M. Nurhuda, K. Midorikawa, Opt. Lett. **33**, 2992 (2008)
11. S. Akturk, C.L. Arnold, B. Zhou, A. Mysyrowicz, Opt. Lett. **34**, 1462 (2009)
12. J. Liu, X.W. Chen, R.X. Li, T. Kobayashi, Laser Phys. Lett. **5**, 45 (2008)
13. O. Varela, A. Zaïr, J. San Román, B. Alonso, I.J. Sola, C. Prieto, L. Roso, Opt. Express **17**, 3630 (2009)
14. X. Chen, A. Jullien, A. Malvache, L. Canova, A. Borot, A. Trisorio, C.G. Durfee, R. Lopez-Martens, Opt. Lett. **34**, 1588 (2009)
15. R. Nuter, S. Skupin, L. Bergé, Opt. Lett. **30**, 917 (2005)
16. R. Nuter, L. Bergé, J. Opt. Soc. Am. B **23**, 874 (2006)
17. I.S. Golubtsov, V.P. Kandidov, O.G. Kosareva, Quantum Electron. **33**, 525 (2003)
18. H. Wille, M. Rodriguez, J. Kasparian, D. Mondelain, J. Yu, A. Mysyrowicz, R. Sauerbrey, J.P. Wolf, L. Wöste, Eur. Phys. J., Appl. Phys. **20**, 183 (2002)
19. G. Méchain, C. D'Amico, Y.-B. André, S. Tzortzakis, M. Franco, B. Prade, A. Mysyrowicz, A. Couairon, E. Salmon, R. Sauerbrey, Opt. Commun. **247**, 171 (2005)
20. J. Park, J.-H. Lee, C.H. Nam, Opt. Express **16**, 4465 (2008)
21. G.P. Agrawal, *Nonlinear Fiber Optics*, 3rd edn. (Academic Press, New York, 2001)
22. J. Liu, X. Chen, J. Liu, Y. Zhu, Y. Leng, J. Dai, R. Li, Z. Xu, Opt. Express **14**, 979 (2006)
23. A. Zaïr, A. Guandalini, F. Schapper, M. Holler, J. Biegert, L. Gallmann, A. Couairon, M. Franco, A. Mysyrowicz, U. Keller, Opt. Express **15**, 5394 (2008)
24. S. Akturk, C. D'Amico, M. Franco, A. Couairon, A. Mysyrowicz, Opt. Express **15**, 15260 (2007)
25. C. Ruiz, J. San Román, C. Méndez, V. Díaz, L. Plaja, I. Arias, L. Roso, Phys. Rev. Lett. **95**, 053905 (2005)
26. T.S. Luk Bernstein, T.R. Nelson, A. McPherson, S.M. Cameron, Opt. Lett. **28**, 2354 (2003)
27. R. Ackermann, E. Salmon, N. Lascoux, J. Kasparian, P. Rohwetter, K. Stelmaszczyk, S. Li, A. Lindinger, L. Wöste, P. Bejot, L. Bonacina, J.P. Wolf, Appl. Phys. Lett. **89**, 171117 (2006)
28. Yu P. Raizer, Sov. Phys. **8**, 650 (1966)
29. A. Couairon, A. Mysyrowicz, Phys. Rep. **441**, 47 (2007)